Available online at www.sciencedirect.com
SCIENCE DIRECT
C. R. Physique 7 (2006) 86–98
COMPTES RENDUS PHYSIQUE
http://france.elsevier.com/direct/COMREN/

Superconductivity and magnetism/Supraconductivité et magnétisme

Nucleation of superconductivity and vortex matter in hybrid superconductor/ferromagnet nanostructures

Victor V. Moshchalkov *, Dušan S. Golubović, Mathieu Morelle

INPAC—Institute for Nanoscale Physics and Chemistry, Nanoscale Superconductivity and Magnetism Group, Laboratory for Solid State Physics and Magnetism, KU Leuven, Celestijnenlaan 200D, B-3001 Leuven, Belgium

Available online 19 January 2006

Abstract

We have studied the superconducting $T_c(H)$ phase boundary of an Al superconducting disk with a perpendicularly magnetized dot on top of it. We used cylindrical and triangular dots. The inhomogeneous stray fields generated by these dots strongly affect the $T_c(H)$ line, which now has the highest T_c at a finite applied field. This 'magnetic bias' of the $T_c(H)$ phase boundary depends on the magnetization of the dots. The field inhomogeneity leads to a pronounced modification of the $T_c(H)$ periodicity. The theoretical $T_c(H)$ dependence, calculated in the framework of the Ginzburg–Landau theory, fits our experimental data very well. In a superconducting Pb film with a lattice of Co/Pd magnetic dots, field-induced superconductivity has been investigated. This remarkable effect appears due to the compensation of the returning stray fields of the dots by the applied magnetic field. As a result of the field compensation, the total field under the dots is enhanced, whereas in the areas between the dots the total field is strongly reduced, thus causing the field-induced superconductivity to appear. ***To cite this article: V.V. Moshchalkov et al., C. R. Physique 7 (2006).***

Résumé

Nucléation de la supraconducivté et de la vorticité dans des nanostructure hybrides supraconducteur/ferromagnétique. Nous avons étudié la frontière $T_c(H)$ de la phase supraconductrice d'un disque supraconducteur d'aluminium sur lequel est placé un plot magnétisé perpendiculairement. Nous avons utilisé des plots cylindrqiues et triangulaires. Les champs de fuite inhomogènes créés par ces plots affectent fortement la ligne $T_c(H)$, qui atteint maintenant sa T_c maximale pour un champ appliqué fini. Ce « déplacement magnétique » de la frontière $T_c(H)$ dépend de la magnétisation des plots. L'inhomogénéité du champ induit une modification profonde de la périodicité de $T_c(H)$. La dépendance (théorique) de $T_c(H)$, calculée dans le cadre de la théorie de Ginzburg–Landau, est en très bon accord avec nos données expérimentales. Nous avons étudié la supraconductivité induite par le champ dans une couche supraconductrice de Pb sur laquelle est placée un réseau de plots magnétiques de Co/Pd. Cet effet remarquable semble être dû à la compensation par le champ magnétique appliqué des champs de fuite réentrants des plots. Suite à cette compensation, le champ total sous les plots est augmenté, alors qu'il décroît fortement dans les zones situées entre les plots, ce qui provoque l'apparaition de la supraconductivité induite par le champ. ***Pour citer cet article : V.V. Moshchalkov et al., C. R. Physique 7 (2006).***

Keywords: Superconductivity; Ferromagnetism; Hybrid nanostructures

Mots-clés : Supraconductivité ; Ferromagnétisme ; Nanostructures hybrides

* Corresponding author.
E-mail addresses: Victor.Moshchalkov@fys.kuleuven.be (V.V. Moshchalkov), Dusan.Golubovic@fys.kuleuven.ac.be (D.S. Golubović).

1631-0705/$ – see front matter
doi:10.1016/j.crhy.2005.12.004

1. Introduction

Nanostructuring is a very powerful tool to control the confinement of the superconducting condensate and flux. By optimizing the condensate and flux confinement, the superconducting critical parameters, that is, the critical field and critical current, can be strongly enhanced. In superconductor (S)/ferromagnet (F) hybrid nanostructures, the magnetic system provides a highly inhomogeneous local field, which can be used as a sort of 'magnetic template' for an additional fine tuning of the flux confinement and studies of the nucleation of superconductivity in presence of such an inhomogeneous field.

In general, superconductivity and ferromagnetism are often considered as two antagonistic phenomena. Their interplay at the nano-scale has unveiled a number of new physical phenomena (see [1] and references therein). For example, in Josephson junctions, which contain a thin ferromagnetic layer instead of an insulator, the crossover from the usual 0-state to the π-state, accompanied by the spontaneous appearance of a current and magnetic flux in the absence of an externally applied magnetic field, has been observed [2]. This recent implementation of a π Josephson junction based on a ferromagnetic tunnelling layer has provided the proof of a theoretical prediction formulated nearly three decades ago [3].

The π-state in Josephson junctions is a result of the modifications of the Andreev reflection process brought about by the proximity effect between a superconductor and ferromagnet [4]. However, hybrid superconductor/ferromagnet structures wherein the proximity effect is intentionally prevented by using a sufficiently thick insulating spacer layer between S and F layers, thus making the S/F interaction purely magnetic, have also shown a series of new effects and proven to be a very convenient tool to tailor some properties of superconductors.

In this article we focus on hybrid S/F structures where the S/F interaction is magnetic. More specifically, we investigate hybrid S/F structures which contain perpendicularly magnetized hard ferromagnetic elements in the single domains state. First, the analysis of the nucleation of superconductivity in individual singly connected hybrid S/F structures, including the influence of the symmetry of the dot, is given. Thereafter, the effect of the field induced superconductivity in a superconducting film with an array of magnetic dots with perpendicular magnetization is presented.

2. The onset of superconductivity in superconducting disks with a magnetic dot

In this section we study the superconducting $T_c(H)$ phase boundary of a mesoscopic superconducting disk with a circular perpendicularly magnetized dot on top.

The structure, schematically shown in Fig. 1, consists of an Al disk and a Co/Pd magnetic dot. The dot is separated from the disk by a Si spacer layer, which prevents the development of the proximity effect in the disk. The radius and the thickness of the Al disk are 1.08 μm and 60 nm, respectively, whereas the radius of the dot is $r_d = 270$ nm. The dot consists of ten Co/Pd bilayers with the thicknesses of 0.4 nm and 1 nm, respectively, with a 2.5 nm Pd buffer layer. The thickness of the Si spacer layer is 10 nm [5]. Fig. 2(a) shows an atomic force micrograph of the sample, whereas a scanning electron micrograph is shown in Fig. 2(b).

The sample was prepared using electron beam lithography, thermal and ion beam evaporation followed by lift-off. For details concerning the fabrication process we refer to [6].

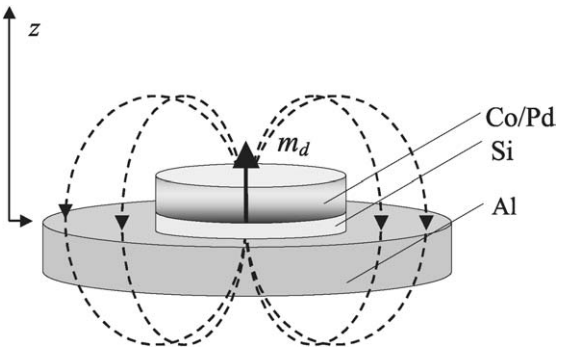

Fig. 1. A schematic of a superconducting disk with the dot on the top.

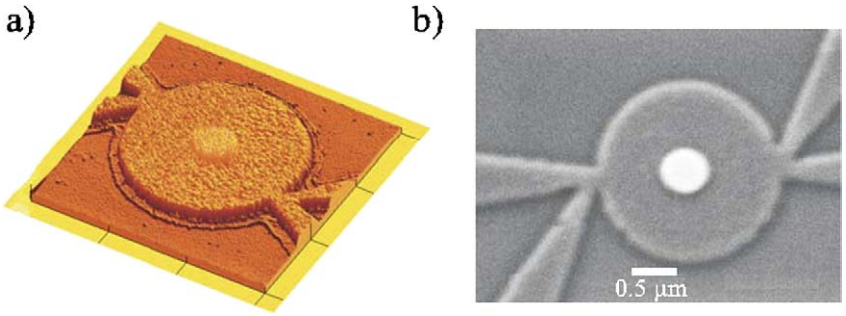

Fig. 2. (a) An atomic force micrograph of the sample and (b) scanning electron micrograph of the sample.

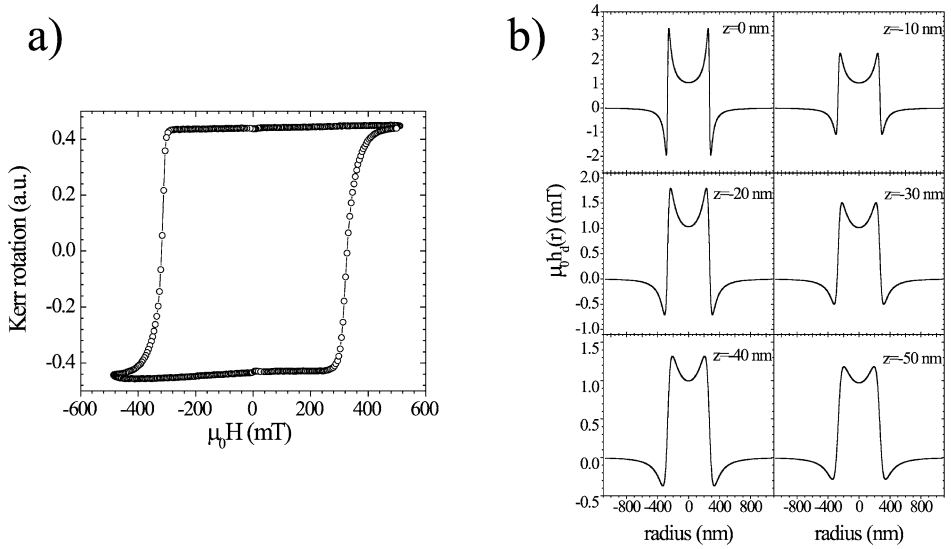

Fig. 3. (a) The room temperature hysteresis loop of the reference Co/Pd film and (b) spatial profiles of the stray field at different positions along the thickness of the disk.

Sub-micrometre Co/Pd magnetic dots are in the single-domain state after saturation in a high magnetic field perpendicular to the sample surface [7]. In the absence of an applied magnetic field, the disk is exposed to the stray field $\vec{h}_d(\vec{r})$ generated by the dot. Assuming that the dot is uniformly magnetized along the z-axis (see Fig. 1) $\vec{m}_d = \vec{i}_z m_d$, the stray field in the cylindrical coordinate system can be expressed as

$$h_d(\vec{r})\vec{i}_z = \frac{\vec{m}_d}{4\pi}\frac{\mathrm{d}^2}{\mathrm{d}z^2}\int \frac{\rho\,\mathrm{d}\rho\,\mathrm{d}\theta\,\mathrm{d}\zeta}{\sqrt{r^2 - 2r\rho\cos(\theta) + (z-\zeta)^2}} \tag{1}$$

whereby the integral is taken over the volume of the dot, ρ, θ and ζ are the coordinates related to the dot, whereas r stands for the radial distance from the centre of the dot and z defines a height with respect to the bottom of the dot. The values of the stray field were calculated assuming that the uniform magnetization of Co layers equals the saturation magnetization of bulk Co ($\mu_0 M_s = 144$ mT) and that the Pd layers are not locally magnetized by the Co layers. The saturation is achieved by exposing a sample to a perpendicular magnetic field higher than the coercive field of Co/Pd, prior to the measurements. For this particular sample, the coercive field of Co/Pd is 300 mT and the dot was saturated in the magnetic field of 800 mT. The room temperature hysteresis loop of the reference co-evaporated Co/Pd film obtained by the magneto-optical Kerr measurements and the stray field profiles at different positions along the thickness of the disk are shown in Fig. 3(a) and 3(b), respectively. Note that in Fig. 1, the position $z = 0$ corresponds to the upper surface of the Al disk. Due to a high aspect ratio radius/thickness of the dot ($r_d/t_d \cong 16$), the stray field is strongly inhomogeneous and sharply peaked at the edges of the dot. The peaks are most pronounced just below and above the dot and gradually decrease farther from the bottom (top) of the dot. Table 1 summarizes the stray

Table 1
The maxima of the positive $\mu_0 h_d^+$ and negative $\mu_0 h_d^-$ stray field in the Al disk

z [nm]	0	−10	−20	−30	−40	−50
$\mu_0 h_d^+$ [mT]	3.300	2.275	1.794	1.508	1.312	1.180
$\mu_0 h_d^-$ [mT]	−1.960	−1.085	−0.706	−0.498	−0.370	−0.284

field values in the Al disk. $\mu_0 h_d^+$ denotes the maximum positive value of the stray field ($\mu_0 h_d(r_d^-)$) and $\mu_0 h_d^-$ the maximum negative value of the stray field ($\mu_0 h_d(r_d^+)$). It is apparent that the stray field has locally very high values. Such high magnetic fields are capable of suppressing superconductivity in the disk, especially very close to the T_{c0} where superconductivity is weak. Given that close to T_{c0} the superconducting coherence length $\xi(T)$ has such values that a spatial variation of the order parameter cannot occur within the disk, it can be anticipated that if the stray field is sufficiently high, superconductivity is completely suppressed in the absence of an applied field and restored by applying a finite external magnetic field. We note that regardless of the high local values of the stray field, the total flux through the Al disk generated by the dot is low and equals $\Phi_m = 0.063$ mT μm^2 or $\Phi_m/\Phi_0 = 0.03$ (Φ_0 is the superconducting flux quantum).

From the resistance of the co-evaporated reference Al bridge at 4.2 K, it was found that the mean free path is $l = 10.5$ nm. The sample is in the dirty limit with the coherence length of $\xi(0) = 110$ nm. Using the value for the London penetration depth of the bulk Al $\lambda_L(0) = 50$ nm, the penetration depth of the sample was estimated $\lambda(0) = 396$ nm, or the GL parameter $\kappa_{\mathrm{GL}} = 3.6$.

Fig. 4 shows the resistive transitions of the sample, taken without an external magnetic field and for the fields of 0.3, 1 and 2 mT, oriented parallel to the magnetization of the dot and 1 and 2 mT oriented antiparallel to the dot. Throughout the article an applied magnetic field parallel to the magnetization of a dot is referred to as positive and vice versa. It can clearly be seen in Fig. 4 that the superconducting disk exhibits the highest critical temperature of 1.42 K, determined using the conventional criterion $R_n/2$ shown by the dashed line ($R_n = 2.8\Omega$ is the residual resistance of the sample), in a finite applied magnetic field of 0.3 mT oriented parallel to the magnetization of the dot. This field is equivalent to $0.53\Phi_0$. The highest critical temperature, hereafter denoted as T_{cm}, is approximately 2 mK higher than the T_{c0}, which is 1.418 K. Given that the temperature resolution of the cryogenic setup is 0.1 mK and the stability 0.2 mK, the difference between T_{cm} and T_{c0} cannot be attributed to noise or temperature instabilities, but to the influence of the dot on the onset of superconductivity.

The critical temperatures for the positive applied fields are systematically higher than the critical temperatures in the same, but oppositely oriented magnetic fields. Table 2 shows the critical temperatures of the sample in positive and negative applied magnetic fields. T_{cp} stands for the critical temperature in a positive applied field, T_{cn} for the corresponding critical temperature in the negative applied field and ΔT_c shows their difference. It turns out that the

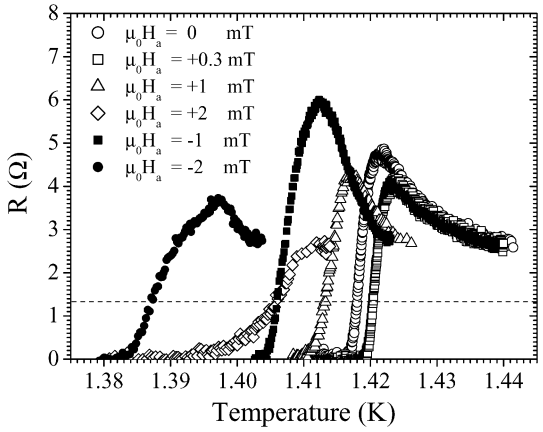

Fig. 4. The resistive $R(T)$ transitions of the structure in zero applied field, +0.3, +1 and +2 mT (open symbols) and −1 mT and −2 mT (filled symbols). The dashed line shows the resistive criterion used.

Table 2
The critical temperatures in the positive applied fields (T_{cp}), negative applied fields (T_{cn}) and their difference $\Delta T_c = T_{cp} - T_{cn}$

$\|B\|$ [mT]	1	2	3	4
T_{cp} [K]	1.4131	1.4057	1.3882	1.3648
T_{cn} [K]	1.4057	1.3871	1.3674	1.3521
ΔT_c [mK]	7.4	18.6	20.8	12.7

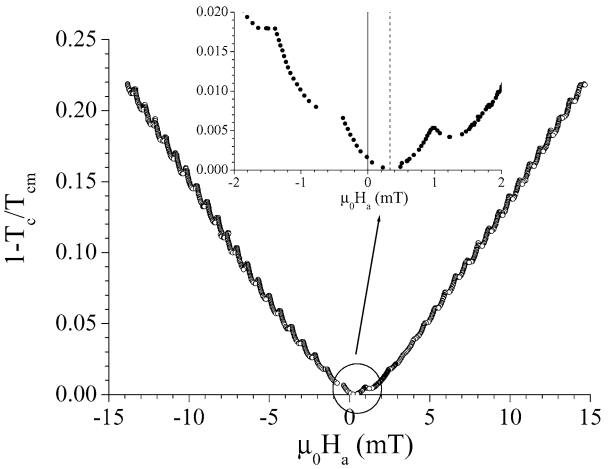

Fig. 5. The superconducting phase boundary of the sample shown as $1 - T_c(H)/T_{cm}$ versus the applied field. The insert shows the phase boundary close to the T_{cm}.

stray field of the dot has such an influence of the onset of superconductivity in the disk, that the critical temperature in a positive applied field approximately equals the critical temperature in 1 mT lower negative field.

The $R(T)$ curves exhibit a pronounced overshoot in the resistance, close to the normal state (see Fig. 4). This excess resistance has already been observed in mesoscopic superconducting samples and is associated with nonequilibrium charge imbalance effects brought about by the non-current-carrying voltage contacts. For details we refer to [8].

Fig. 5 shows the superconducting phase boundary of the sample. The critical temperature $T_c(H)$ of the sample is normalized as $1 - T_c(H)/T_{cm}$. The measurements were taken down to 1.1 K, with the field and temperature step of 40 μT and 0.5 mK, respectively. The lock-in technique was used with a transport current of 150 nA and the frequency 27.7 Hz. The inset show the phase boundary in the vicinity of T_{cm}. The phase boundary, in agreement with the $R(T)$ measurements, exhibits a shift along the field axis. The maximum critical temperature of 1.421 K is attained at 0.33 mT or $0.58\Phi_0$. The seeming discrepancy between the $R(T)$ and phase boundary measurements is just a result of different resolutions of these measurements. Given the steps in the field and temperature in the $T_c(H)$ measurements, they are undoubtedly more accurate and reliable. The $T_c(H)$ phase boundary has a linear background, which is the hallmark of the nucleation of superconductivity in a singly connected (2D) structure.

The experimental $T_c(H)$ phase boundary has been analyzed in the framework of Ginzburg–Landau (GL) theory.[1] The GL equations were solved numerically, without introducing any constraints to the form of the order parameter, that is, a giant vortex state (GVS), as well as all other combinations involving individual Φ_0-vortices or a combination of a GVS and Φ_0-vortices were allowed. It was assumed that there was no screening so that the total magnetic field is

$$\mu_0 \vec{H} = \mu_0 H_a \vec{i}_z + \mu_0 h_d(r) \vec{i}_z \tag{2}$$

The vector potential was, therefore, taken as

$$\vec{a}(r) = \frac{\mu_0 H_a r}{2} \vec{i}_\theta + a_d(r) \vec{i}_\theta \tag{3}$$

[1] The calculations have been performed by M.V. Milošević.

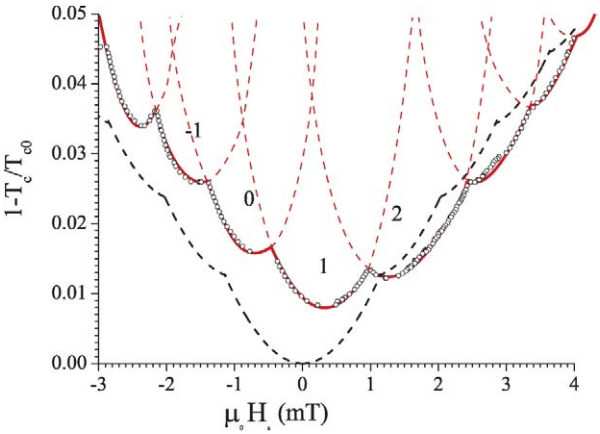

Fig. 6. The superconducting phase boundary of the sample shown as $1 - T_c(H)/T_{cm}$ versus the applied field $\mu_0 H_a$. The symbols are the experimental data, the solid line is the theoretical curve obtained using the numerical approach and the dashed line is the theoretical phase boundary of the disk without the dot. The numbers indicate the vorticity.

whereby $\mu_0 \vec{h}_d(r) = \nabla \times \vec{a}_d(r)$ was obtained numerically. The magnetization of the bulk Co was used in the calculations. The $T_c(H)$ phase boundary was obtained using the real dimensions of the Al disks and dot, as obtained from the atomic force microscopy, whilst keeping the coherence length as the free parameter, since the contacts were not included in the model. The Neumann boundary condition for the order parameter was used.

Fig. 6 shows the experimental data together with theoretical curves for the phase boundary of the disk with the dot, given by the solid line, and an identical disk without the dot, displayed by the dashed line. The numbers indicate the vorticity. The calculations were performed down to 1.35 K. The best agreement between the theory and experiment was achieved with the coherence length $\xi(T) = 102$ nm.

The calculations have revealed that the vorticity of the GVS induced by the stray field of the dot equals one. The comparison with the $T_c(H)$ phase boundary of the reference disk without the dot shows that the stray field reduces the zero-field critical temperature, in this particular case by 1.5%, as well as that the critical field of the disk with the dot is enhanced in positive applied fields. In addition to the shift along the field axis, the calculations show that the dot modifies the phase boundary along the temperature axis in that it breaks the mirror symmetry of the $T_c(H)$ phase boundary with respect to the maximum critical temperature. The inhomogeneity of the stray field has been identified as the main reason for the modification of the phase boundary along the temperature axis. If an Al disk were exposed to a constant, but homogeneous, magnetic field, the phase boundary would be shifted along the field axis according to the polarity of the additional field. The maximum critical temperature T_{cm} would be achieved for a finite value of the applied field which completely compensates the additional field. In the case of the complete compensation, the total flux in the disk would be equal to zero and the T_{cm} would be equal to the T_{c0} of an equivalent disk which is not exposed to the additional magnetic field. For this reason, the mirror symmetry of the phase boundary would be retained. The $T_c(H)$ phase boundary would not be an even function with respect to $\mu_0 H_a = 0$, as in the case of a reference disk, but would be an even function with respect to the applied field which compensates the additional field. In other words, the $T_c(H)$ phase boundary would simply be translated along the field axis.

The inhomogeneous stray field generated by a dot cannot be cancelled out by applying any homogeneous field. Therefore, in an Al disk with a magnetic element there is always a finite flux which brings about a reduction in the zero-field critical temperature, shown in Fig. 6. In addition to a reduction of the T_{c0}, which may have been anticipated using very simple arguments, the pronounced inhomogeneity of the stray field and the modification of the $T_c(H)$ phase boundary along the temperature axis, are also reflected in different contributions of a change in the applied field of $\mu_0 \Delta H_a$ close to T_{c0}, or equivalently T_{cm} as these are close to each other, and at lower temperatures. For instance, a change in the applied magnetic field from $\mu_0 H_a = 0$ to $\mu_0 H_a = \pm 0.1$ mT, changes the total flux in the Al disk, but the peak values of the stray field (see Table 1) remain high. Given that the superconducting coherence length is much greater than the radius of the disk, substantial spatial variations of the order parameter in the disk are penalized and the order parameter cannot follow the spatial profile of the stray field. Therefore, even though the total flux in the disk is low, superconductivity can be completely suppressed in the disk if the stray field is sufficiently high. The

phenomenon that a spatially localized magnetic field actually governs the onset of superconductivity in the whole structure is peculiar to individual hybrid S/F structures and is a direct consequence of the confinement of the order parameter.

Higher values of the applied field are sufficient to reduce the peak values of the stray field and the onset of superconductivity is predominantly governed by the total flux, which is more similar to the onset of superconductivity in a uniform magnetic field. This crossover from the field to flux dominance in the nucleation of superconductivity is induced by the inhomogeneity of the stray field and the confinement of the superconducting condensate and is the origin of the broken evenness of the $T_c(H)$ phase boundary.

3. Symmetry effects in hybrid superconductor/ferromagnet systems

Symmetry is known to have a major impact on the nucleation of superconductivity in mesoscopic structures. In superconducting mesoscopic samples with cylindrical symmetry, like disks and loops, the onset of superconductivity close to the T_{c0} occurs in the form of a GVS [9,10]. As long as the superconducting coherence length is greater than the radius of the disk, the symmetry of the boundary makes the cylindrically symmetric distribution of the order parameters energetically more preferable than any combination of individual Φ_0-vortices. For sufficiently low temperatures and/or big disks, a GVS state splits into a collection of individual Φ_0-vortices, which may even, if disks are sufficiently big, recover the triangular Abrikosov configuration [11]. On the other hand, superconducting micro- and nanostructures structures with reduced symmetry exhibit a substantially different behaviour. In superconducting squares, with the C_4 axial symmetry, a GVS may not be the lowest energy state close to the phase boundary [12]. A nonuniform distribution of the order parameter, caused by the presence of sharp corners where the superconductivity is enhanced, favors the nucleation in the form of individual Φ_0-vortices [12–14]. For example, the state with the vorticity $L = 2$ consists of two vortices, which are aligned parallel to the edges of the square at higher temperatures and rearrange to lie on a diagonal of the square, for lower temperatures [13,14]. When the vorticity switches to $L = 3$, any configuration of three Φ_0-vortices cannot conform to the symmetry imposed by the boundaries of the square. Therefore, just as a result of the mismatch between the possible arrangements of three Φ_0-vortices and the C_4 symmetry of the square a vortex-antivortex pair appears [12,14]. The antivortex is located at the centre of the square, whereas four vortices are located at the diagonals of the square. The same effect has been observed in a mesoscopic superconducting triangle [15]. In this case, a vortex-antivortex pair nucleates for the vorticity $L = 2$ in order to comply with the imposed C_3 symmetry.

In order to establish how the symmetry of the stray field generated by a perpendicularly magnetized magnetic dot affects the nucleation of superconductivity, a superconducting disk with a triangular magnetic dot, hereafter referred to as the triangle, has been investigated [16]. Unlike in the case of a disk with a circular magnetic dot where both the superconductor and magnetic element are cylindrically symmetry, for a disk with a triangular dot there is an apparent difference in the symmetry of the superconducting boundary and the symmetry of the stray field.

A scanning electron micrograph of the sample is shown in Fig. 7. The 30 nm thick Al disk has the radius of 1.34 μm and contains a Co/Pt triangle on the top. Even though the triangle was designed as equilateral, its sides are 690, 650

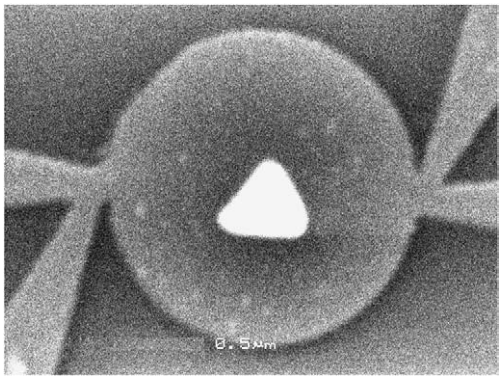

Fig. 7. A scanning electron micrograph of the sample.

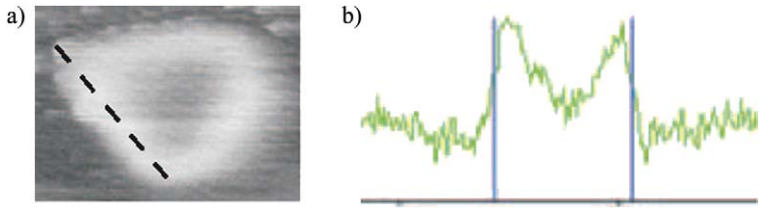

Fig. 8. A magnetic force micrograph of the triangle (a) and the spatial profile of the magnetic force on the tip (b). The dashed line shows the direction along which the magnetic force was measured.

and 740 nm. The Co/Pt triangle consists of a 2.5 nm Pt buffer layer a 10 bi-layers of Co and Pt with the thicknesses of 0.4 and 1 nm, respectively. The coercive field of the co-evaporated reference film is 170 mT at room temperature, with a 90% remanence. Prior to the measurements the dot was saturated in the magnetic field of 600 mT applied perpendicularly to the sample surface. The triangle is separated from the superconducting disk by a 4 nm Si spacer layer to avoid the proximity effect.

Fig. 8(a) shows a magnetic force micrograph of the triangle, whereas Fig. 8(b) shows the spatial profile of the magnetic force on the magnetic tip. The dashed line in Fig. 8(a) shows the direction along which the force was recorded. The triangle is clearly in the single domain state. Brighter contrast along the edges indicates the area of a higher stray field.

The $T_c(H)$ phase boundary was obtained in exactly the same way as explained above. The temperature and field steps were 0.5 mK and 50 μT, respectively. The room temperature resistance and the residual resistance at 4.2 K of the sample are 6.5 and 3.2Ω, respectively. The mean free path of Al, estimated from the co-evaporated transport bridge, is 12.3 nm, so that the sample is a type II-superconductor in the dirty limit with the coherence length $\xi(0) = 120$ nm. The penetration depth is $\lambda(0) = 365$ nm or the GL parameter $\kappa_{\mathrm{GL}} = 3.04$. The critical temperature of the sample in zero applied field is $T_{c0} = 1.4136$ K.

The critical temperature $1 - T_c/T_{cm}$ of the sample versus the applied magnetic field $\mu_0 H_a$ down to 1.25 K is shown in Fig. 9. As with the circular magnetic dot, the phase boundary is shifted along the field axis and the maximum critical temperature $T_{cm} = 1.4155$ K is achieved for the applied field of 0.1835 mT or $0.48\Phi_0$. The $T_c(H)$ phase boundary has the typical cusp-like behaviour for negative applied fields. The cusps are strongly suppressed for the positive applied fields in the range $1.43 \leqslant \mu_0 H_a \leqslant 3.25$ [mT], then reappear and remain visible down to 1.25 K. The range of the positive magnetic field wherein no cusps are observed corresponds to $4.95\Phi_0$.

An Al disk without the triangle was prepared as the reference simultaneously with the disk containing the triangle. The phase boundary of the reference disk, with $T_{c0} = 1.4366$ K, is shown in Fig. 10. As the $T_c(H)$ phase boundary of the reference disk exhibits the typical cusp-like behaviour, the absence of the cusps in the $T_c(H)$ phase boundary

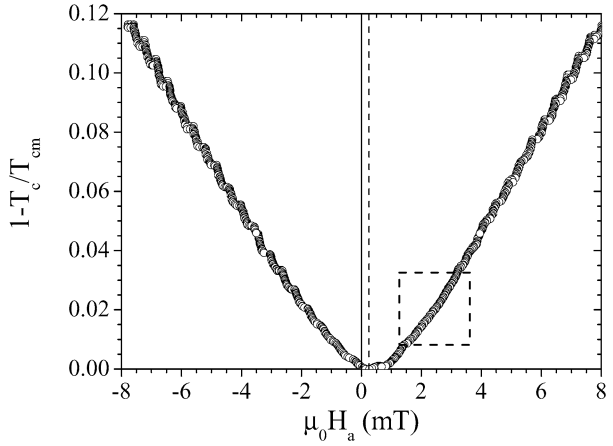

Fig. 9. The superconducting $T_c(H)$ phase boundary of the disk with the triangle.

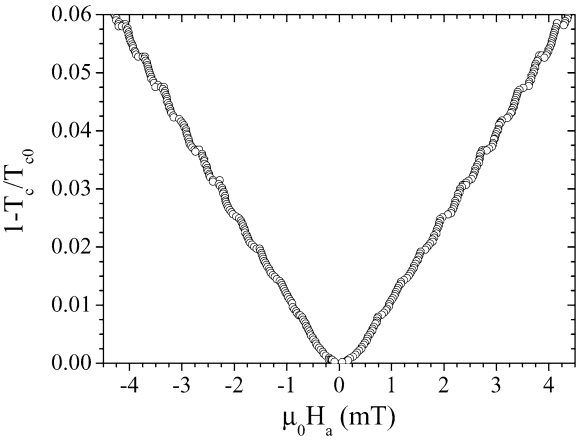

Fig. 10. The superconducting $T_c(H)$ phase boundary of the reference Al disk without the triangular magnetic dot.

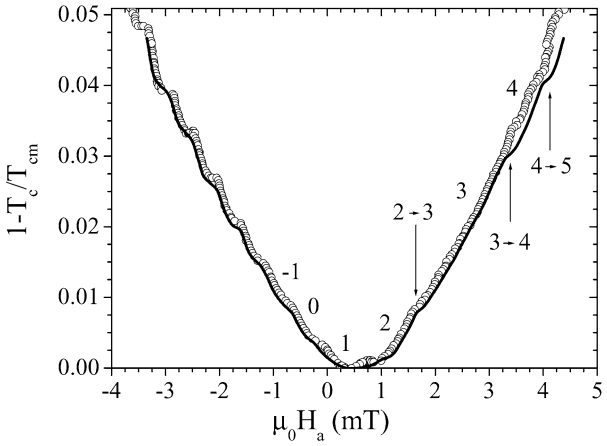

Fig. 11. $T_c(H)$ phase boundary of a superconducting disk with a magnetic triangle. The solid line presents the theoretical curve, whereas open symbols show experimental data. Numbers stand for the vorticity, with arrows indicating the transitions between the states with different vorticities (after Ref. [16]).

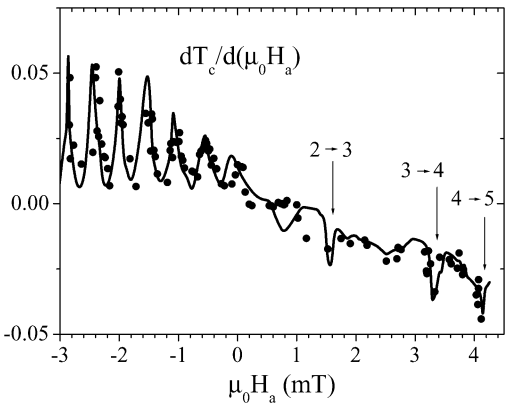

Fig. 12. The first derivative of the critical temperature with respect to the applied magnetic field. Filled symbols are the experimental data and solid line is the theoretical curve.

of the disk with the triangle cannot be attributed to some unusual, preparation related, properties of the samples, or contacts. It is clear that the features of the phase boundary in Fig. 9 are brought about by the presence of the triangle, which generates an additional highly inhomogeneous stray field.

The experimental results have been analyzed using the Ginzburg–Landau equations solved numerically, as described in the previous section, down to 1.35 K. In order to make the calculations as accurate as possible, the current and voltage contacts were modelled by adding two stripes to the disk at positions of the contacts in the sample. The real dimensions of the disk and triangle, as obtained by atomic force microscopy, were used, whereas the length and width of the stripes were taken to be 400 nm and 250 nm, respectively. Even though the sample has wedge shaped contacts, the strips are considered to adequately model their influence, because they allow a local outspread of the current, as well as provide a local enhancement of superconductivity, which in the real sample comes from the non-current-carrying voltage contacts. The stray field was calculated assuming that the magnetization of the Co layers equals the saturation magnetization of Co and the coherence length was kept as the free parameter [16]. The best agreement between the theory and experiment was obtained for $\xi(0) = 118$ nm, which is just 1.5% lower than the experimental value of the coherence length.

Fig. 11 shows the experimental data (open symbols) and theoretical curve (solid line), displayed as $1 - T_c/T_{cm}$ versus the applied field $\mu_0 H_a$. In Fig. 12 the first derivative of the critical temperature $\mathrm{d}T_c/\mathrm{d}(\mu_0 H_a)$ versus the applied field is given. The vorticity in zero field equals one, which implies that the extended cusp in the $T_c(H)$ phase boundary corresponds to the vorticity $L = +3$ of the order parameter. Given that the stray field has the C_3 symmetry, a pronounced field stability of the vorticity $L = +3$ seems to be related to the competition between different symmetries of the superconducting disk and the triangle.

In Fig. 13 the field range $\Delta\Phi_L$ over which a particular vorticity is stable is shown for the disk with a circular dot, analyzed in Section 3.3, and the disk with the triangle. The figure is plotted as $\Delta\Phi_L/\Phi_0$ versus the vorticity L. Open symbols are used for the disk with the circular dot and filled symbols are used for the disk with the triangular dot. The lines are just a guide to the eye. It is clear that the only major difference in the nucleation of superconductivity occurs for $L = +3$. In the disk with the triangle, this vorticity remains stable in a broad range of applied magnetic fields, whereas all other vorticities have the stability range typical for mesoscopic superconducting disks at the phase boundary [10].

When there is one vortex in the disk ($L = +1$), it is located at the centre of the triangle. The entrance of the second vortex ($L = +2$) does not alter the distribution of the order parameter as the two vortices merge forming a GVS. However, the appearance of the third vortex ($L = +3$) brings about a substantial redistribution of the order parameter within the disk. The GVS breaks into three individual Φ_0-vortices and the three vortices assume the positions below the apices of the triangle. Given that the stray field of the triangle is the highest at its apices, the three Φ_0-vortices are

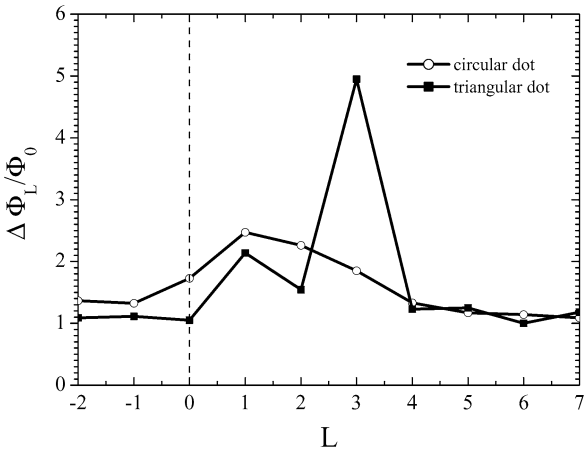

Fig. 13. The field ranged $\Delta\Phi_L$ over which a vorticity L is stable. Open symbols are used for the disk with the dot and filled symbols for the disk with the triangle. The lines are a guide to the eye.

strongly pinned and this configuration remains stable in a broad range of fields and temperatures. The fourth vortex in the disk ($L = +4$) does not lead to a reconfiguration of the triangular vortex pattern—the three vortices remain located at the apices, whereas the fourth vortex moves to the centre of the triangle. Upon the entry of the fifth vortex ($L = +5$), the three Φ_0-vortices remain pinned at their original positions. The fifth vortex merges with the vortex at the centre of the triangle and they form a GVS with the vorticity $+2$. The entrance of the sixth vortex ($L = +6$) causes another reconfiguration of the vortex pattern and a GVS with the vorticity $+6$ is formed at the centre of the triangle. This comes about as the stray field of the dot is not sufficient to hold two vortices, either as a GVS with the vorticity $+2$ or two individual Φ_0-vortices, at the apices of the triangle and the GVS below the triangle is energetically more favorable. We describe this behaviour as a symmetry induced reentrant behaviour at the phase boundary. The splitting of a GVS state into a collection of Φ_0-vortices and a merger of Φ_0-vortices into a GVS in a mesoscopic superconducting disk at the phase boundary is essentially new and peculiar. As mentioned above, as long as the temperature is sufficiently high and the superconducting coherence length is greater than the radius of a disk, the onset of superconductivity occurs through a GVS state. At lower temperatures, the GVS can split into a collection of individual vortices, which can assume various spatial configurations. However, this transition is irreversible in sense that once a GVS has split into Φ_0-vortices and the temperature is further decreased, states consisting of individual Φ_0-vortices become energetically more favorable over the GVS and, thus, more stable. In the case of the Al disk with the triangle, the GVS becomes unfavorable at approximately 0.993 T_{cm} and then reappears as the most favorable at roughly 0.943 T_{cm}, remaining stable down to the lowest measured temperature of 1.25 K.

This is a clear indication that there is a profound competition between the symmetries of the disk and triangle, which has an impact on the nucleation of superconductivity. The symmetry of the triangle comes into play because the triangular profile of the stray field induces an extremely inhomogeneous distribution of the screening currents in the disk. Namely, when a circular dot is placed on top of a disk the screening currents induced by the stray field and an applied field, regardless of its polarity, are cylindrically symmetric. The total current in the disk, therefore, inherently follows the symmetry imposed by the boundary of the disk and a GVS is the lowest energy state close to the phase boundary. On the other hand, the triangle induces a screening current of the same symmetry in the disk. Furthermore, the stray field of the triangle is additionally inhomogeneous compared to a circular dot, because the field values at the apices are higher than along the edges. Therefore, the total screening current in the disk can be thought of as though it consists of two components—one component whirls around the triangle and the other component is localized at the positions of the apices. Hence, the interaction between the screening current induced by the triangle and a cylindrically symmetric screening current generated by an applied magnetic field is non-trivial and its outcome cannot be easily conjectured using simple arguments. However, numerical simulations carried out on this system for magnetic polygons confirm that a GVS splits into a collection of Φ_0-vortices whenever the vorticity of a GVS equals the number of apices of a polygon, that is, for $L = +4$ in the case of a Co/Pt square, for $L = +5$ in the case of a Co/Pt pentagon and so forth [17].

4. Field induced superconductivity

Some superconducting materials are not only able to withstand magnetic fields, but to have superconductivity that can even be induced by applying a magnetic field. Such materials are very rare and up to now only (EuSn)Mo_6S_8, $HoMo_6S_8$, and organic λ-$(BETS)_2FeCl_4$ compounds show this unusual behavior [18,19]. The appearance of the magnetic-field-induced superconductivity (FIS) in these compounds was interpreted in terms of the Jaccarino–Peter effect, in which the exchange fields from the paramagnetic ions compensate an applied magnetic field, so that the destructive action of the field is neutralized [20].

FIS can also be realized in hybrid superconductor/ferromagnet nanostructured bilayers. The basic idea is quite straightforward (see Fig. 14): a lattice of magnetic dots with magnetic moments aligned along the perpendicular direction is placed on top of a superconducting film. The magnetic stray field of each dot has a positive component of the magnetic induction B_z under the dots and a negative one in the area between the dots. Added to a homogeneous magnetic field H, see Fig. 14(b)), these dipole fields enhance the component of the effective magnetic field $\mu_0 H_{\text{eff}} = \mu_0 H + B_z$ in the small area just under the dots and, at the expense of that, reduce H_{eff} elsewhere in the Pb film, thus providing the condition necessary for the FIS observation. This new field compensation effect is not restricted to specific superconductors, so that FIS could be achieved in any superconducting film with a lattice of magnetic dots.

This idea has been implemented by using a thin superconducting film with an array of magnetic dots on top. The sample consists of a 85 nm superconducting Pb film evaporated on a 1 nm Ge base layer on an amorphous Si/SiO_2 substrate. This thin Pb-film behaves as a type-II superconductor. For protection against oxidation, the Pb is covered by a 10 nm Ge layer that is insulating at low temperatures and thus prevents the influence of the proximity effect between Pb and Co/Pd. The Ge/Pb/Ge trilayer is patterned into a transport bridge (width 200 μm, distance between voltage contacts 630 μm) using optical lithography and chemical wet etching. The ferromagnetic dots are made by defining a resist mask on the transport bridge by electron-beam lithography and subsequent evaporation of a Pd(3.5 nm)/$[Co(0.4\text{ nm})/Pd(1.4\text{ nm})]_{10}$ multilayer into the resist mask. The resist is finally removed in a lift-off procedure. The dots are arranged in a regular square array with period 1.5 μm. They have a square shape with the side length of about 0.8 μm.

The H–T-phase boundary separating the normal (N) from the superconducting state is clearly altered by changing the magnetic state of the dot array, as shown in Fig. 15. A conventional symmetric (with respect to H) phase boundary is obtained when $m = 0$. Two kinks in the curve can be seen at $H = \pm H_1$, with H_1 the first matching field $\mu_0 H_1 = \Phi_0/(1.5\ \mu\text{m})^2 = 0.92$ mT, at which the applied flux per unit cell of the dot array is exactly one superconducting flux quantum Φ_0. In contrast to that, the H–T-phase boundary is strongly asymmetric with respect to H when the dots are magnetized. Moreover, the maximum T_c is shifted to $+2H_1$ when the magnetization of the dots and the applied field are parallel and to $-2H_1$ when they are antiparallel. Thus, the shift gives rise to FIS when dots are magnetized.

In the present system, the FIS can be explained by taking into account the local magnetic induction of the dots **B**, as schematically indicated in Fig. 14. In the absence of an applied magnetic field the magnetic dipoles generate stray fields exceeding the upper critical field of the Pb film when $T > 7.185$ K, and, as a result, the Pb film is in the normal state. In an applied field of $H = +H_2$, the compensation of B_z takes place in the interdot area where the Pb

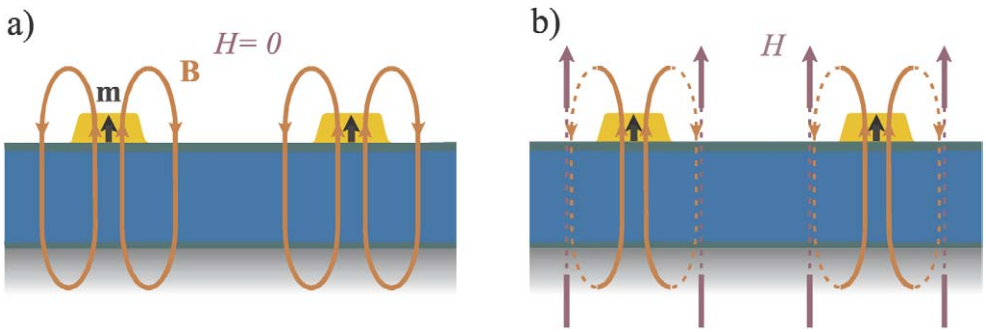

Fig. 14. A schematic of the hybrid superconductor/ferromagnet sample with FIS. (a) The magnetic stray field B of the dots is comparable with the field of a magnetic dipole. (b) A magnetic field H applied in the perpendicular direction can be compensated by the dipole stray field between the dots, resulting in the conditions necessary for the observation of magnetic field-induced superconductivity.

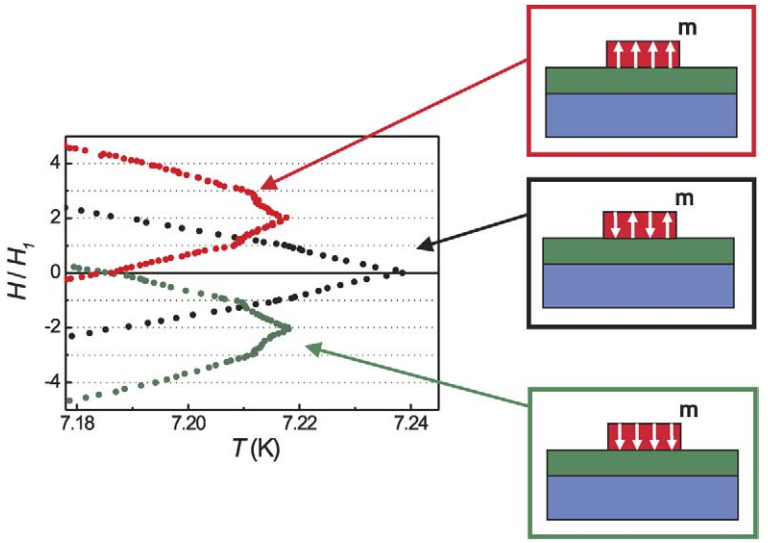

Fig. 15. The magnetic field (H)–temperature (T)-phase diagrams of the Pb film for the three magnetic states of the dots. These data are derived from $\rho(T)$-measurements carried out in a Quantum Design Physical Properties Measurement System applying a 4-probe ac technique with an ac-current of 10 μA at a frequency of 19 Hz. H is applied perpendicular to the sample surface. We defined the critical temperature as $T_c = T$ ($\rho = 50\%\rho_n$), with ρ the resistivity and $\rho_n = 1.4$ μΩ cm the normal state resistivity at 7.3 K. H_1 is the first matching field.

film is now in the superconducting state, thus providing the percolation through dominantly superconducting areas, and making possible the continuous flow of Cooper pairs and zero film resistance.

An important feature to note here is the appearance of periodic kinks in the H–T-phase boundary with a period coinciding with the first matching field H_1, caused by the fluxoid quantization. The maximum T_c at exactly $H = +2H_1$ can therefore be understood in terms of fluxoid quantization: the flux created by the stray field between the dots can be estimated from the magnetostatic calculations to be about $-2.1\Phi_0$ per unit cell of the dot array. This makes $H = +2H_1$ a favorable field for fulfilling the fluxoid quantization constraint. Similar arguments can also be applied for the dots magnetized antiparallel to the applied field to explain the shift of the maximum T_c to $H = -2H_1$. For $m = 0$, **B** is strongly reduced due to the domain structure in the dots. This means that the stray field only weakly influences the Pb film, leading to a phase boundary without peculiarities except the weak kinks at $H = \pm H_1$.

5. Conclusion

For individual S/F nanostructures (S-disk with a cylindrical F-dot and S-disk with a triangular F-dot) we have found very pronounced effects of the inhomogeneous local fields generated by the dots on the onset of the superconducting state. The symmetry of these local fields also plays an important role, as we deduced from the essential difference in the periodicity of the cusp in the $T_c(H)$ phase boundaries of Al disks with triangular and cylindrical magnetic dots. Finally, a lattice of Co/Pd has been used as a nanoengineered magnetic field compensator to enhance substantially the critical field for a given fixed polarity and also observe field-polarity dependent field-induced superconductivity. The studied S/F hybrid nanostructures have clearly demonstrated the possibility of optimizing the superconducting critical parameters with the help of magnetic field templates produced by magnetic nanosystem in S/F hybrids.

Acknowledgements

The authors would like to extend their thanks to M. Lange for his contribution and useful discussions, M.V. Milošević and F.M. Peeters for the theoretical results and A. Volodin for AFM and MFM measurements. This work has been supported by the Research Fund K.U. Leuven GOA/2004/02 programme, the Flemish FWO and the Belgian IUAP programmes, as well as by the JSPS/ESF "Nanoscience and Engineering in Superconductivity" programme.

References

[1] I.F. Lyuksytov, V.L. Pokrovsky, Adv. Phys. 54 (2005) 67;
A.I. Buzdin, Rev. Mod. Phys 77 (2005) 935.
[2] V.V. Ryazanov, V.A. Oboznov, A.Y. Rusanov, A.V. Veretennikov, A.A. Golubov, J. Aarts, Phys. Rev. Lett. 86 (2001) 2427;
S.M. Frolov, D.J. Van Harlingen, V.A. Oboznov, V.V. Bolginov, V.V. Ryazanov, Phys. Rev. B 70 (2004) 144505;
A. Bauer, J. Bentner, M. Aprili, M.L. Della Rocca, M. Reinwald, W. Wegscheider, C. Strunk, Phys. Rev. Lett. 92 (2004) 217001.
[3] L.M. Bulaevskii, V.V. Kuzii, A.A. Sobyanin, Solid State Commun. 25 (1978) 1053.
[4] A. Buzdin, A.E. Koshelev, Phys. Rev. B 67 (2003) 220504;
A. Buzdin, I. Baladie, Phys. Rev. B 67 (2003) 184519;
Z. Radović, N. Lazarides, N. Flytzanis, Phys. Rev. B 67 (2003) 014501;
T. Yokoyama, Y. Tanaka, A.A. Golubov, J. Inoue, Y. Asano, Phys. Rev. B 71 (2005) 094506.
[5] D.S. Golubović, W.V. Pogosov, M. Morelle, V.V. Moshchalkov, Europhys. Lett. 65 (2004) 546;
D.S. Golubović, W.V. Pogosov, M. Morelle, V.V. Moshchalkov, Physica C 404 (2004) 182.
[6] D.S. Golubović, W.V. Pogosov, M. Morelle, V.V. Moshchalkov, Phys. Rev. B 68 (2003) 172503.
[7] M. Lange, M.J. Van Bael, Y. Bruynseraede, V.V. Moshchalkov, Phys. Rev. Lett. 90 (2003) 197006.
[8] M. Morelle, Y. Bruynseraede, V.V. Moshchalkov, Phys. Stat. Solid. B 237 (2003) 365;
C. Strunk, et al., Phys. Rev. B 57 (1998) 10854.
[9] V.A. Schweigert, F.M. Peeters, Phys. Rev. Lett. 83 (1999) 2409.
[10] V. Bruyndoncx, L. Van Look, M. Verschuere, V.V. Moshchalkov, Phys. Rev. B 60 (1999) 10468.
[11] A.K. Geim, S.V. Dubonos, J.J. Palacios, I.V. Grigorieva, M. Henini, J.J. Schermer, Phys. Rev. Lett. 85 (2000) 1528;
L.R.E. Cabral, B.J. Baelus, F.M. Peeters, Phys. Rev. B 70 (2004) 144523.
[12] L.F. Chibotaru, A. Ceulemans, V. Bruyndoncx, V.V. Moshchalkov, Nature 408 (2000) 833.
[13] A.S. Mel'nikov, I.M. Nefedov, D.A. Ryzhov, I.A. Shereshevskii, V.M. Vinokur, P.P. Vysheslavtsev, Phys. Rev. B 65 (2002) 140503.
[14] J. Bonča, V.V. Kabanov, Phys. Rev. B 65 (2002) 012059;
T. Mertelj, V.V. Kabanov, Phys. Rev. B 67 (2003) 134527.
[15] L.F. Chibotaru, A. Ceulemans, V. Bruyndoncx, V.V. Moshchalkov, Phys. Rev. Lett. 86 (2001) 1323.
[16] D.S. Golubović, M.V. Milošević, F.M. Peeters, V.V. Moshchalkov, Phys. Rev. B 71 (2005) 180502(R).
[17] M.V. Milošević, private communication.
[18] S.A. Wolf, et al., Phys. Rev. B 25 (1982) 1990;
H.W. Meul, et al., Phys. Rev. Lett. 53 (1984) 497;
M. Giroud, et al., J. Low Temp. Phys. 69 (1987) 419.
[19] S. Uji, et al., Nature 410 (2001) 908;
L. Balicas, et al., Phys. Rev. Lett. 87 (2001) 067002.
[20] V. Jaccarino, M. Peter, Phys. Rev. Lett. 9 (1962) 290.